Applied Mathematical Sciences, Vol. 1, 2007, no. 11, 527 - 550

Weak Majorization as an Approach to Non-Equilibrium Foam Decay

S. Sauerbrei [1], K. Knicker, E. C. Hass, P. J. Plath [2]

Institut für Angewandte und Physikalische Chemie
AG Chemische Synergetik
Universität Bremen, Bibliothekstrasse NW2
D-28359 Bremen, Germany

Abstract

Defined initial conditions are assumed for foam measurements. Especially, the frothing up method influences the foam decay. We like to show the influence of the frothing up method with ultrasound on beer foam which depends on the vessel size and liquid beer height.

Foam pictures are evaluated by measuring the bubble sizes which are then represented by normalized bubble size distributions (histograms). In [7, 8] we have seen that decaying foam with its histograms can be characterized by the classical majorization [4, 2, 1, 3], that means histograms can be described by statistical order or incomparableness. We have mapped bubble size histograms on the Shannon entropy [9] and obtained a complex time development of this entropy. Now we like to take into account the diminishing number of bubbles during foam decay by means of the weak submajorization [3] in order to get a more realistic description. The structure of the weak submajorization can be represented with partition diagram lattices [5] and influenced by permuting and normalizing of this partition diagrams.

Keywords: Foam Decay; Majorization; Diagram Lattices

1 Experiment

Our measurements show a linear dependence of the liquid height l_{liq} of the non-foamed beer and the maximum height of the resulting foam $l_{foam,max}$, using the frothing up method with ultrasound.

For this beer foam experiments we take *Warsteiner* beer at 24±1°C. Pouring carefully different volumes V_{liq} (the volume V_{liq} is increased in 10 ml steps)

[1] sonja@uni-bremen.de
[2] plath@uni-bremen.de

of the non-foamed beer in measuring cylinders of different diameters d (d=2.6, 3.0, 3.6, 3.9, and 5.0 cm). The minimal and maximum non-foamed liquid beer volumes of the measuring cylinders can be seen in Table 1. These liquid vol-

Table 1: The minimal (min) and maximum (max) non-foamed liquid beer volumes of the measuring cylinders d=2.6, 3.0, 3.6, 3.9, and 5.0 cm.

d [cm]	2.6	3.0	3.6	3.9	5.0
min [ml]	10	10	10	10	20
max [ml]	50	50	110	130	250

umes V_{liq} are frothed up with ultrasound (Ultrasonik 28x; NEY) for 13 s until there is no more increase in foam volume V_{foam}. After frothing up the maximum foam volume $V_{foam,max}$ and its decay time t (defined to be the time t until the foam layer collapses and the liquid surface becomes visible from above) are measured. To take into account the different sized measuring cylinders, we divide both the liquid volume V_{liq} before frothing up and the maximum foam volumes $V_{foam,max}$ by the corresponding diameter d of the measuring cylinder and obtain the liquid height l_{liq} and foam height $l_{foam,max}$ by (1)

$$l_{liq} = \frac{4V_{liq}}{d^2\pi} \qquad \text{and} \qquad l_{foam,max} = \frac{4V_{foam,max}}{d^2\pi}. \tag{1}$$

In Fig. 1 we see the maximum foam height $l_{foam,max}$ plotted against the liquid height l_{liq} to show the linear relationship between these variables as a result of this frothing up method with ultrasound.

In Fig. 2 we see the decay time t of the maximum foam height $l_{foam,max}$ plotted against the original liquid height l_{liq} for the measuring cylinder with d=3.6 cm being representative of all used measuring cylinder sizes. A linear behaviour is found for small liquid heights l_{liq}. This behaviour changes for high initial liquid heights l_{liq}, in which case the foam column comes close to the rim of the measuring cylinder. This experimental founding leads one to conjecture that the functional behaviour of the decay time t depends on the CO_2 atmosphere in the measuring cylinder above the foam surface. In case of low initial liquid heights l_{liq} and thus smaller maximum foam heights $l_{foam,max}$ the air in the free column of the measuring cylinder becomes enriched in CO_2 due to the CO_2-release from bursting bubbles. For larger initial liquid heights l_{liq} and thus higher maximum foam heights $l_{foam,max}$ the foam column comes close to the rim of the measuring cylinder and the gas exchange with the surrounding air above the measuring cylinder is faciliated, probably leading to lower CO_2 partial pressures just above the foam column. In this case the foam decay becomes faster and the linear relationship between the liquid heitght l_{liq} and decay time t no longer holds (Fig. 2).

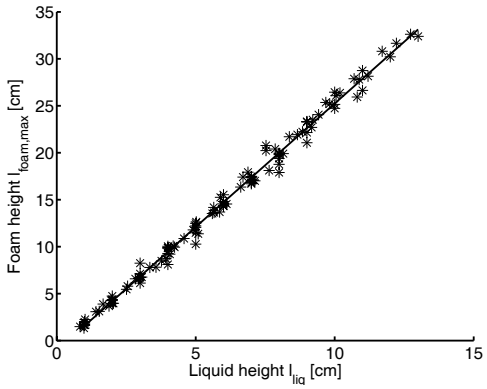

Figure 1: The linear relationship between maximum foam height $l_{foam,max}$ and liquid height l_{liq} is based on the frothing up method with ultrasound. The plot refers to all measuring cylinders we have mentioned in this section. Note that the maximum foam height and liquid height are expressed by the measuring cylinder diameters, see (1).

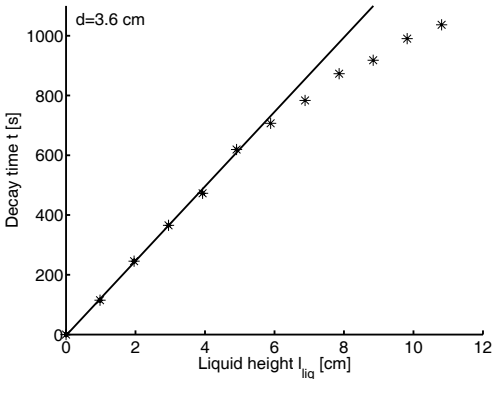

Figure 2: The plot of the foam decay time t against the original liquid height l_{liq} for the measuring cylinder with $d = 3.6$ cm being representative of all used measuring cylinder sizes. Clearly, the deviation of the linear function can be considered for high initial liquid heights l_{liq} which develops high foam columns coming close to the rim of the measuring cylinder.

We summarize that the linear behaviour of the decay time t of small liquid heights l_{liq}, where the resulting foam surface of the maximum foam height $l_{foam,max}$ is far enough away from the cylinder opening to preserve a high enough partial pressure of CO_2 over the foam surface.

If the foam surface of the maximum foam height $l_{foam,max}$ approximates to the cylinder opening, the partial pressure of CO_2 in the atmosphere will decrease and the partial pressure difference between CO_2 in the bubbles and CO_2 atmosphere will increase. An increasing partial pressure difference leads to stronger gas exchange between bubbles and atmosphere and the foam decay becomes faster.

Furthermore, we take pictures of the foam decay to examine the bubble size distributions (histograms) of this pictures. The experimental set-up is described in section 4. But firstly, we introduce the mathematics which we like to apply to the histograms in the following section.

2 Majorization

The classical majorization of Muirhead, Hardy, Littlewood and Polya [4, 2] is defined by (2) and (3) saying that γ majorizes γ'

$$\gamma' \prec \gamma \qquad if \qquad \sum_{1}^{k} \gamma'_{[i]} \leq \sum_{1}^{k} \gamma_{[i]}, \qquad k = 1, \cdots, n-1, \tag{2}$$

and

$$\sum_{i=1}^{n} \gamma'_i = \sum_{i=1}^{n} \gamma_i. \tag{3}$$

Let $\gamma, \gamma' \in \mathbb{R}^n$ and let $\gamma = (\gamma_{[i]})$ denotes a positive semidefinite vector rearranged in nonincreasing order ($\gamma_1 \geq \gamma_2 \geq \cdots \geq \gamma_n$). If γ majorizes γ' ($\gamma' \prec \gamma$) then there exists a doubly stochastic matrix D such that $D\gamma = \gamma'$. And a real-valued function Φ is said to be Schur-concave if

$$\gamma' \prec \gamma \qquad \text{then} \qquad \Phi(\gamma') \geq \Phi(\gamma). \tag{4}$$

The concept of the weak majorization which we have mentioned in [8] can be expressed by (5) and (6) for the weak submajorization [3]:

$$\gamma' \prec_w \gamma \qquad if \qquad \sum_{1}^{k} \gamma'_{[i]} \leq \sum_{1}^{k} \gamma_{[i]}, \qquad k = 1, \cdots, n, \tag{5}$$

and

$$\sum_{i=1}^{n} \gamma'_i \leq \sum_{i=1}^{n} \gamma_i, \tag{6}$$

where $\gamma = (\gamma_{[i]})$ is a positive semidefinite vector whose components are rearranged in nonincreasing order. Then γ weakly submajorizes γ', $\gamma' \prec_w \gamma$ and there exists a doubly substochastic matrix P such that $P\gamma = \gamma'$. And a real-valued function Φ satisfies

$$\gamma' \prec_w \gamma \qquad \text{then} \qquad \Phi(\gamma') \leq \Phi(\gamma) \tag{7}$$

if and only if Φ is increasing and Schur-convex. For more details with regard to majorization in general see the fundamental work of P. M. Alberti, A. Uhlmann [1] and of A. W. Marshall, I. Olkin [3].

A special modification of the majorization is the partial sum comparison without rearranging vectors in order to take into account the permutation of the vectors. This type of majorization we have described in [8].

3 Classical Majorization and Weak Submajorization Represented by Diagram Lattices

A discrete representation of the classical majorization and order of the classical majorization respectively are Ruch's diagram lattices [5] which are based on partitions of an integer n. If one goes from the lowest upper bound *lub* to the greatest lower bound *glb* along these lattices, the diagrams obey the classical majorization, that means transitions in this direction (represented by arrows, see Fig. 3) between the diagrams indicate doubly stochastic matrices D (8), see Fig. 3.

$$\text{If} \quad \gamma \to \gamma', \quad \text{then} \quad \gamma \succ \gamma' \quad \text{and} \quad D\gamma = \gamma'. \tag{8}$$

Clearly diagrams can be characterized by vectors [8] (Fig. 5). These vectors consist of a number of boxes denoted by n and are embedded in a vector space of a dimension that is denoted by i.

The weak submajorization makes possible trace change of the vectors. Strictly speaking the trace of the vector can decrease (6) (the trace *tr* of a vector is the sum of its components). For our discrete approach, trace changing means for example transitions between the $n = 6$ and the $n = 5$ diagram lattice. In other words, there are $n = 6$ diagrams which weakly submajorize $n = 5$ diagrams.

The transitions of the weak submajorization (represented by scatterd arrows) correspond to doubly substochastic matrices P (9).

$$\text{If} \quad \gamma \dashrightarrow \gamma', \quad \text{then} \quad \gamma \succ_w \gamma' \quad \text{and} \quad P\gamma = \gamma'. \tag{9}$$

Fig. 4 shows the transitions of the classical majorization (arrows) and the weak submajorization transtitions (scattered arrows) of the $n = 6$ and $n = 5$ diagrams. It is easy to see $n = 6$ diagrams which contain one box in the lowest row weakly submajorize $n = 5$ diagrams by elimination of this single box. In Fig. 4 the $n = 6$ and $n = 5$ partition diagrams of the same level (that means a horizontal line in the diagram lattice) are incomparable. (Ruch lattices with $n \geq 6$ [5] are partially ordered sets.) In our work [8] we have represented diagrams with n boxes as vectors which are extended with zero elements to obtain vectors of the dimension $i = n$, see Fig. 5 on the left. Additionally, these vectors can be permuted, see Fig. 5 on the right. Each partition diagram lattice posses a certain number of permutations which can be computed by the formula of combination with replacement (10)

$$C_{n,i} = \binom{n+i-1}{i} = \binom{2n-1}{n} = \frac{(2n-1)!}{n!(n-1)!}, \tag{10}$$

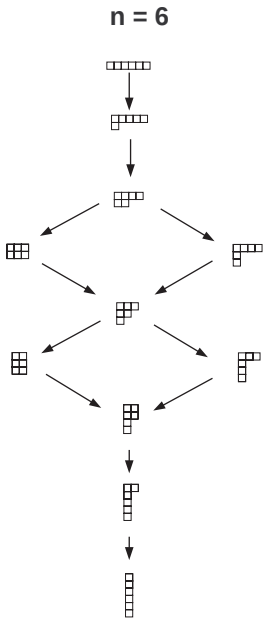

Figure 3: The $n = 6$ Ruch diagram lattice. The arrows characterize the direction from *lub* to *glb* and the transitions (doubly stochastic matrices D (8)) between the diagrams.

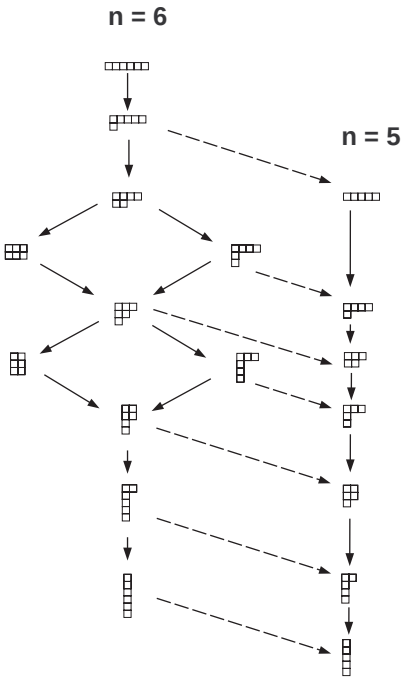

Figure 4: The $n = 6$ and $n = 5$ diagram lattice with classical majorization transitions (arrows or doubly stochastic matrices D (8)) and weak submajorization transitions (scattered arrows or doubly substochastic matrices P (9)). The arrows characterize the direction from *lub* to *glb*.

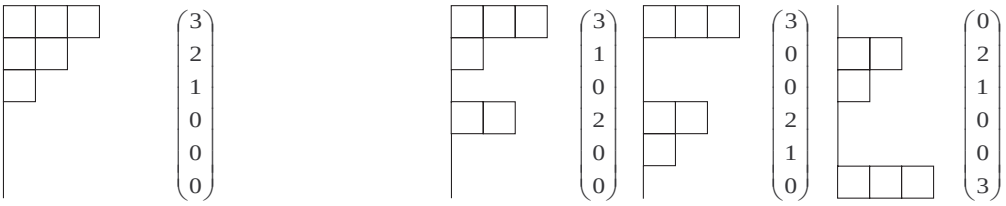

Figure 5: On the left an $n = 6$ diagram with its corresponding vector of the dimension $i = 6$ that is equal to number of boxes $n = 6$ extended with zero elements. On the right some permutations of this diagram with its corresponding vectors.

with $i = n$ [10]. Now, we consider the weak submajorization in Fig. 4. To calculate the transitions of the weak submajorization (scatterd arrows) by (5) one sets the dimension $i = 6$ for both the $n = 6$ and $n = 5$ diagrams and vectors respectively because the vectors have to belong to the same vector space of the dimension i, see section 2. That means the number of permutations of the $n = 5$ diagram lattice increases owing to the increased dimension $i = 6$ instead of the dimension $i = 5$, that we would use for the classical majorization. To obtain the number of permutations for $n \neq i$ one has to take the expression (11)

$$C^{\star}_{n,i} = \binom{n+i-1}{i-1}. \tag{11}$$

It is easy to see that

$$C_{n,i} = C^{\star}_{n,i} \qquad \text{for} \qquad n = i. \tag{12}$$

We like to proof (12):

$$\text{if} \quad \binom{n+i-1}{i} = \binom{n+i-1}{i-1} \tag{13}$$

$$\overset{n=i}{\Leftrightarrow} \quad \binom{2n-1}{n} = \binom{2n-1}{n-1} \tag{14}$$

$$\overset{\binom{n}{i}=\frac{n!}{(n-i)!i!}}{\Leftrightarrow} \frac{(2n-1)!}{(2n-1-n)!n!} = \frac{(2n-1)!}{(2n-1-(n-1))!(n-1)!} \tag{15}$$

$$\Leftrightarrow \frac{(2n-1)!}{(n-1)!n!} = \frac{(2n-1)!}{n!(n-1)!}. \tag{16}$$

In Table 2 the number of permutations of n with different dimensions i is shown. This Table 2 is comparable to the Pascal triangle. We see that for our above mentioned example the number of permutations of the $n = 5$ diagrams doubles if the dimension changes from $i = 5$ to $i = 6$ (bold numbers). Fig. 6 gives an example for number of permutations of $n = 3$ diagrams and their frameworks for different embedding dimensions i (or different number of rows). The frameworks can be generated by a modification of the classical majorization shown in detail in [8]. These structures of permuted partition diagrams (***p**artition-**p**ermutation-structures*, abbreviated *pp-structures* [8]) can be combined with the weak submajorization. To obtain these structures we

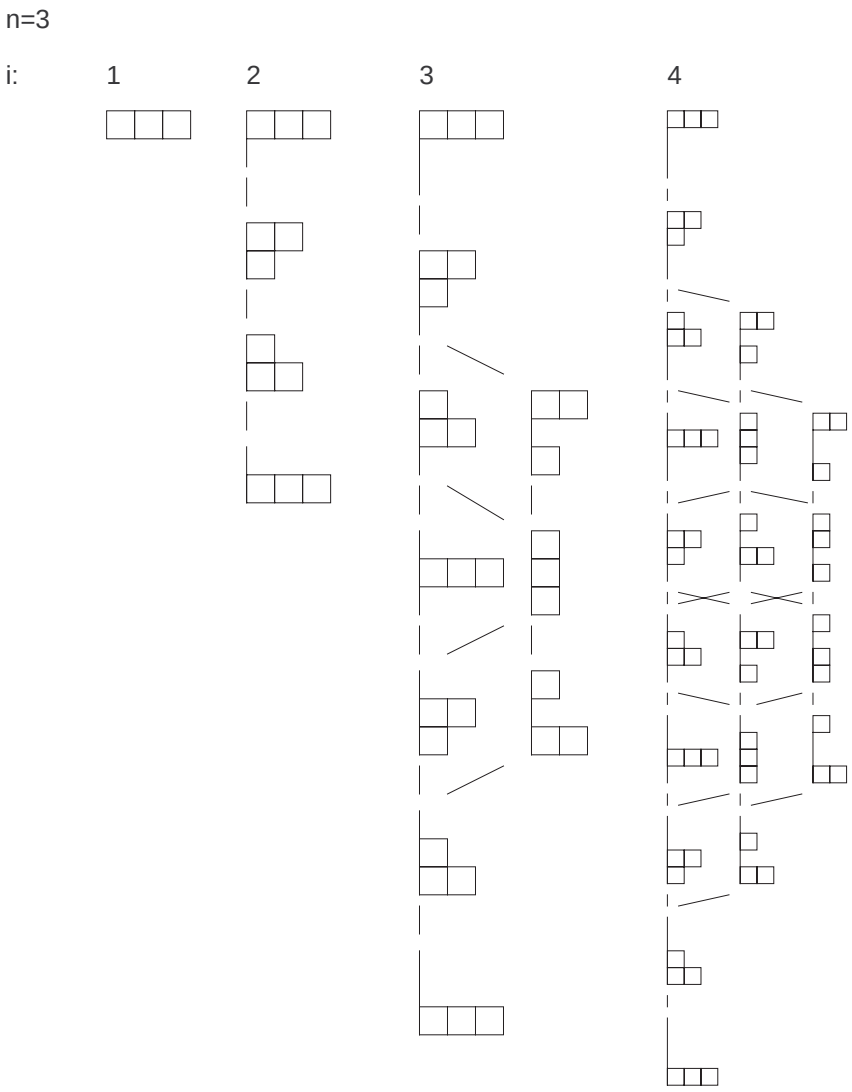

Figure 6: The frameworks of the $n = 3$ diagrams for different number of rows i (different embedding dimensions i) generated by the modification of the classical majorization [8].

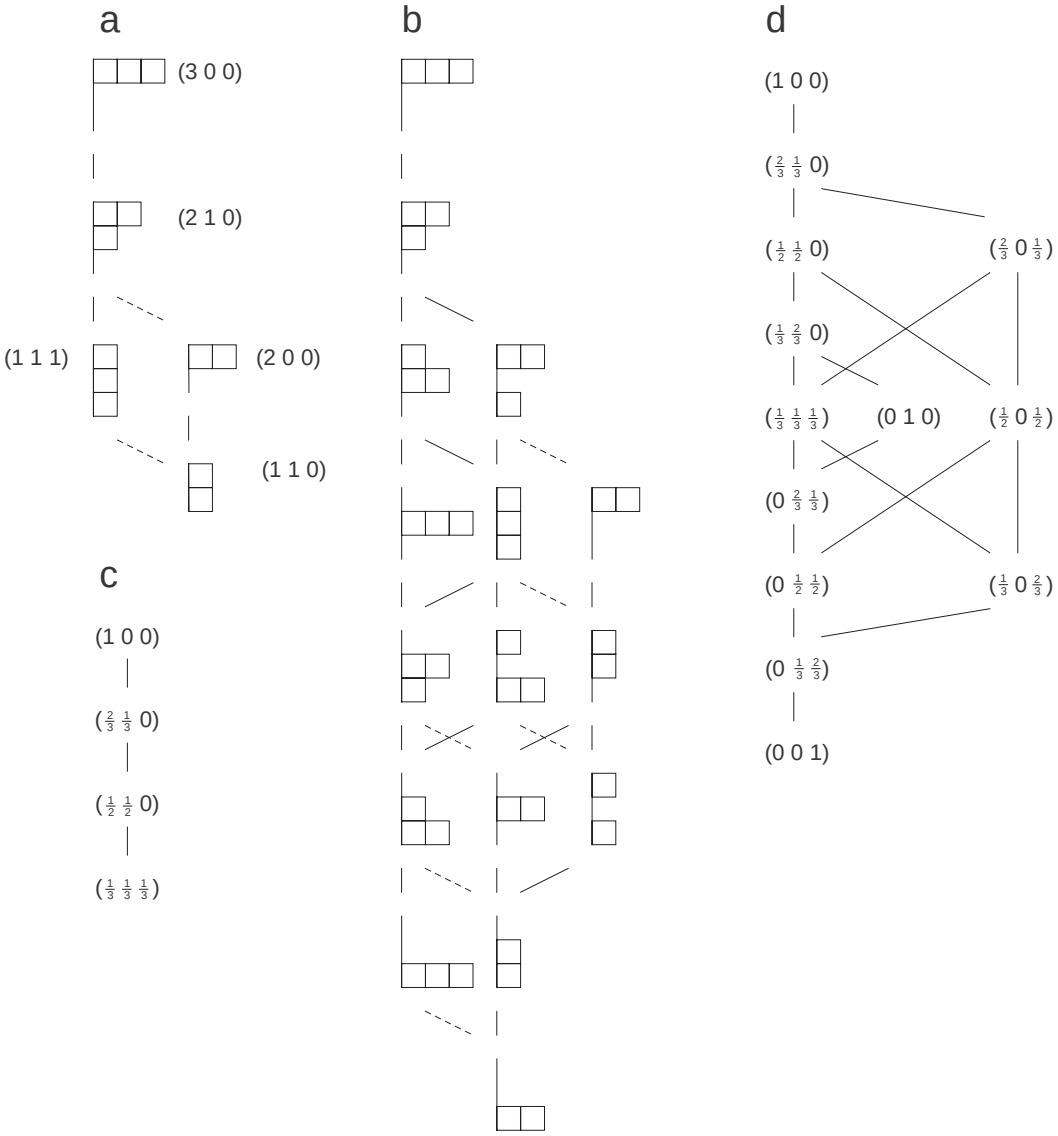

Figure 7: **a**: the $n = 3$ and the $n = 2$ Ruch lattice with the dimension $i = 3$ joined by the weak submajorization (scattered lines); **b**: the *pp-structures* of $n = 3$, $i = 3$ diagrams and $n = 2$, $i = 3$ diagrams joined by the weak submajorization (scattered lines); **c**: the totally ordered structure which originates from the structure in **a** after normalizing the diagrams; **d**: the relations of the diagrams in **b** after normalizing.

Table 2: The number of permutations of partitions of an integer n with different dimensions i which can be generated by (11). This Table is comparable to the Pascal triangle.

	n	0	1	2	3	4	5	6
i								
1		1	1	1	1	1	1	1
2		1	2	3	4	5	6	7
3		1	3	6	10	15	21	28
4		1	4	10	20	35	56	84
5		1	5	15	35	70	**126**	210
6		1	6	21	56	126	**252**	462

use the modification of the classical majorization [8]. In Fig. 7 (b) the transitions of the weak submajorization between the $n = 3$, $i = 3$ diagrams and the $n = 2$, $i = 3$ diagrams are shown (scattered lines). Additionally, we see the framework of the $n = 3$ and the $n = 2$ diagrams without permutations Fig. 7 (a) (compare to Fig. 4). In contrast to the transitions shown in Fig. 4 in Fig. 7 (b) one box of the lowest row is removed, however this row can contain even more than one box, it does not need to contain only one single box.

3.1 Incomparableness

Partition diagrams as vectors can be normalized to unity. Normalization makes possible the join of the $n = 6$ and the $n = 5$ diagram lattices in Fig. 4. The resulting structure shows clear differences refering to their diagram order, see Fig. 8 and compare to Fig. 4. Changing diagram order means that the mathematical relations of the majorization also change. In the following comparison we will refer to the framework in Fig. 4 and consider the changing relations after normalizing (Fig. 8). Firstly, the relations which do not change are the order of the majorization and incomparableness in the classical sense: if two $n = 6$ diagram vectors a and b are incomparable or a majorizes b ($b \prec a$) then this relation does not change after normalizing and joining with the $n = 5$ diagram vectors. Suppose an $n = 6$ diagram vector a weakly submajorizes an $n = 5$ diagram vector x ($x \prec_w a$). However, these vectors a, x as normalized vectors a_{norm}, x_{norm} behave differently: x_{norm} majorizes a_{norm} ($a_{norm} \prec x_{norm}$).

An interesting case are the lowest upper bounds of the $n = 6$ and $n = 5$ diagram lattices. These diagram vectors are equivalent as normalized vectors. Then there are $n = 6$ diagram vectors a, b and a majorizes b ($b \prec a$). Additionally, the $n = 6$ diagram vectors b weakly submajorizes a $n = 5$ diagram

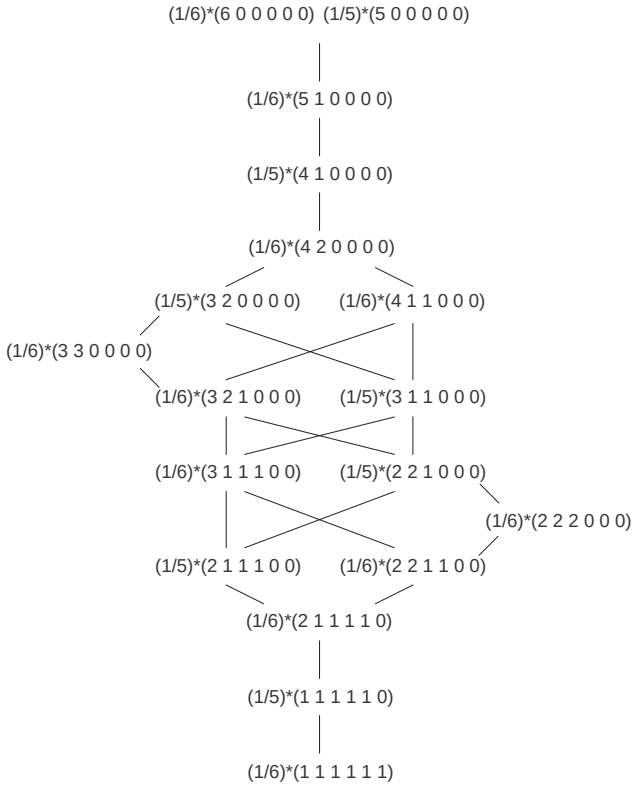

Figure 8: Join of the $n = 6$ and the $n = 5$ diagrams and vectors respectively by normalizing. The structure obeys the classical majorization.

vector x ($x \prec_w b \prec a$). The corresponding normalized vectors a_{norm}, b_{norm}, x_{norm} can behave as follows: a_{norm} is incomparable to x_{norm}, a_{norm} majorizes b_{norm} (no change) and x_{norm} majorizes b_{norm} ($a_{norm} \succ b_{norm} \prec x_{norm}$).

We see that permuting and normalizing of diagrams and diagram vectors influences the frameworks, that means the ordering of the diagrams changes. As an overview, see Fig. 7: **a**: the classical majorization and the weak submajorization (scattered lines) without permutations of the $n = 3$ and the $n = 2$ diagrams of the dimension $i = 3$; **b**: the *pp-structure* of (a) generated by the modification of the majorization; **c**: the join of the diagrams in (a) by normalizing the diagram vectors (classical majorization); **d**: the *pp-structure* of (c) (modification of majorization). It is clear for (c) and (d) that diagram vectors like (3 0 0) and (2 0 0) and their corresponding permutations after normalizing are equal and consequently the number of diagrams and diagram vectors respectively changes.

We take the example of the $n = 3$ and the $n = 2$ diagrams with the dimension $i = 3$ due the number of diagrams and diagram vectors respectively. The example of the $n = 6$ and $n = 5$ diagrams is interesting because of the partial order of the original $n = 6$ diagram lattice, but for the *pp-structures* these diagrams are not suitable because the structure can be hardly illustrated (the *pp-structure* with the weak submajorization of the $n = 6$ and the $n = 5$ diagrams with the dimension $i = 6$ consists of 714 diagrams, see Table 2).

4 Histograms and Majorization

After frothing up the beer with ultrasound mostly small bubbles are present. While the foam is shrinking, different processes influence the bubble sizes. At the end of the rearrangement, there are few very large bubbles which replace many small ones [6]. This bubble size development causes the decreasing number of bubbles of constant sized bubble pictures. In Fig. 9 we see only small bubbles after frothing up and in Fig. 10 the large and small bubbles at the end of the rearrangement. The picture frame is constant in Figs. 9, 10, but it is clear that there are absolutely more bubbles in Fig. 9 than in Fig. 10.

The foam pictures are taken with a CCD-camera (CV-M10 CCD camera; lens 0.5×; framesize 1.3×1.0 cm). For illumination, a cold light source (KL 2500 LCD) is used. 20 ml *Warsteiner* beer is frothed up with ultrasound for 13 s in a rectangular glass vessel (2.5×2.5 cm). Here, it is important to know that the behaviour of the decaying foam does not change using a rectangular glass vessel instead of a measuring cylinder. Pictures are being taken in 10 s intervals. The bubble sizes defined by their bubble diameter d are divided into ten size intervals with a width of 1.73 10^{-4} m (the last interval is open). We are convinced that for description of our system this chosen interval division is optimal. For each bubble size interval a relative frequency p_i is

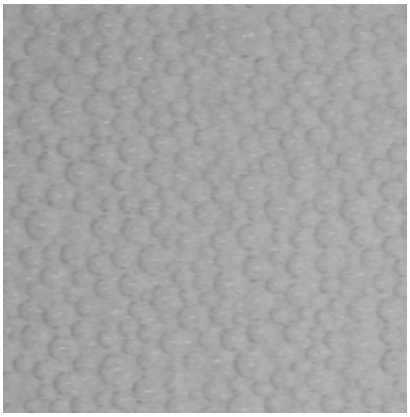

Figure 9: A large number of small bubbles after frothing up the beer with ultrasound.

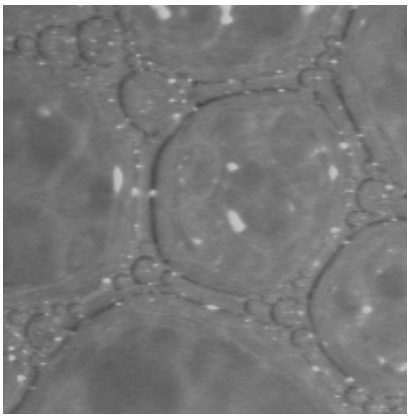

Figure 10: The number of bubbles is diminished due to the development of large bubbles.

given to examine the temporal development of the bubble size distributions $h(t) = (p_i(t))$ (Fig. 11) in terms of statistics by means of majorization, see section 2. The bubble size distributions $h(t) = (p_i(t))$ are dependent on time vectors whose entries are denoted by p_i. To compare the distributions vectors $h(t) = (p_i(t))$ by means of the majorization these vectors are rearranged in decreasing order: $(p_1 \geq p_2 \geq \cdots \geq p_n)$. For simplicity the notation of $p_i(t)$ is identically with p_i. More experimental details are given in [8].

In Fig. 12 the decreasing number of bubbles of constant sized foam pictures is shown. We consider the normalized bubble size distributions $h(t) = (p_i(t))$ with $\sum_{i=1}^{10} p_i = 1$ by means of the classical majorization (2), (3) and the bubble size distributions with a decreasing number of bubbles $\sum_{i=1}^{10} p_i \leq 1$ by means of the weak submajorization (5), (6).

The classical majorization characterizes the temporal development of the normalized bubble size distributions $h(t) = (p_i(t))$ as follows: $h(10\ s) \succ h(20\ s) \succ h(30\ s) \succ h(40\ s) \succ h(50\ s) \succ h(60\ s) \succ h(70\ s) \succ h(80\ s) \nsim h(90\ s) \nsim h(100\ s) \succ h(110\ s) \nsim h(120\ s) \nsim h(130\ s) \nsim h(140\ s) \nsim h(150\ s) \nsim h(160\ s) \prec h(170\ s) \prec h(180\ s) \prec h(190\ s) \prec h(200\ s) \nsim h(210\ s) \nsim h(220\ s) \succ h(230\ s) \nsim h(240\ s) \nsim h(250\ s)$. It is noteworthy that most of the bubble size distributions are incomparable, denoted by '$\nsim$'. In section 3.1 we have seen that if two vectors a, b are incomparable, $a \nsim b$, then there exists a vector x which majorizes (is majorized by) a and b: $a \prec x \succ b$ $(a \succ x \prec b)$. If we express the classical majorization in terms of statistical order, we see that at the beginning from 10 s to 80 s the statistical order diminishes or the *mixing character* increases (Ruch 1975 [5]). In other words, if distribution vector a majorizes (is majorized by) distribution vector b, $a \succ b$ $(a \prec b)$ then the statistical order decreases (increases) from a to b. In this case our bubble

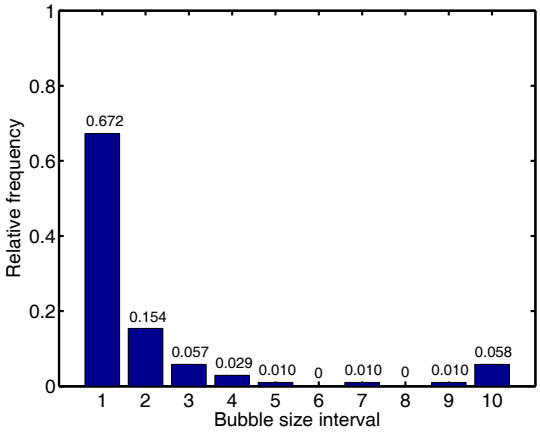

Figure 11: Normalized bubble size distribution $h(t) = (p_i(t))$ after $t = 200\ s$ with the relative frequencies $p_i(t)$ above the columns whose sum is one, $\sum_{i=1}^{10} p_i(t) = 1$.

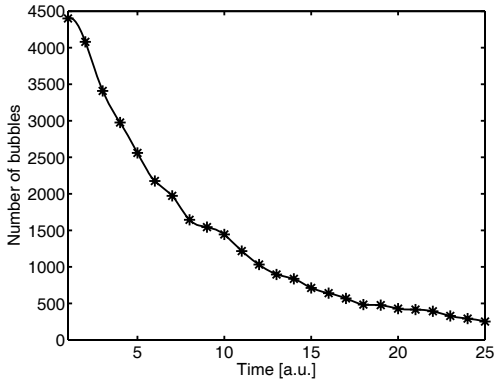

Figure 12: Temporal development of the decreasing number of bubbles of constant sized foam pictures.

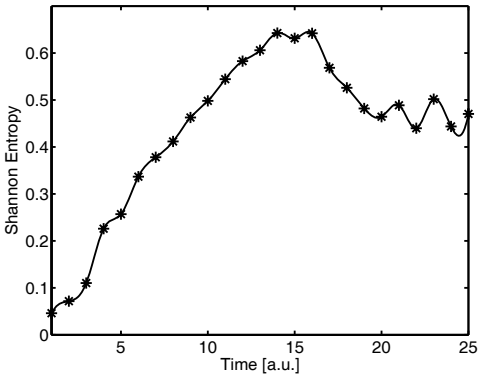

Figure 13: Temporal development of the Shannon entropy (17) of the normalized bubble size distributions $h(t) = (p_i(t))$.

size distributions follow an ordinary diffusion process as one would usually expect in terms of the classical thermodynamics. From 160 s to 200 s there are unexpectedly transitions which describe an increasing statistical order. This increasing order corresponds to the unstable structure formation of the *Apollonian* package [6]. The transitions of incomparable bubble size distributions consists of increasing and decreasing statistical order, but if two distribution vectors a, b are incomparable $a \nsim b$ one does not know whether the increasing statistical order or the decreasing statistical order predominates.

Of course, we can map the histograms $h(t) = (p_i(t))$ in the traditional way on the Shannon entropy [9] for a better examination of the temporal development of the statistical order. The normalized Shannon entropy [6] is calculated by (17)

$$I(h(t)) = -\frac{1}{\log_2 n} \sum_{i=1}^{n} p_i(t) \log_2 p_i(t), \tag{17}$$

where $p_i(t)$ denotes the relative frequencies of the bubble sizes and n the number of size intervals, here is $n = 10$. Then

$$a \succ b \quad \text{implies} \quad I(a) \leq I(b). \tag{18}$$

The temporal development of the classical majorization relations of the bubble size distributions represented by the Shannon entropy (17) can be seen in Fig. 13. We see the Shannon entropy (17) increases from 10 s to 140 s (here the process of drainage is described [8]) and then it begins to behave irregularly (here the process of rearrangement is described [8]). This can be related to the decreasing number of bubbles during the foam decay which are not taken into account by normalizing the bubble size distributions. The weak majorization (5), (6) takes the decreasing number of bubbles during foam decay into consideration. To apply the weak submajorization we can take the absolute bubble number of the bubble size intervals or later we normalize in a way that all absolute bubble size distribution are divided by the maximum number of bubbles of the first bubble size distribution in order to obtain special kind of 'relative frequencies' which we call weak frequencies p_i with $\sum_{i=1}^{10} p_i \leq 1$.

The resulting relations of the temporal development of the bubble size distribution in terms of the weak submajorization are given by: $h(10\ s) \succ_w h(20\ s) \succ_w h(30\ s) \succ_w h(40\ s) \succ_w h(50\ s) \succ_w h(60\ s) \succ_w h(70\ s) \succ_w h(80\ s) \succ_w h(90\ s) \succ_w h(100\ s) \succ_w h(110\ s) \succ_w h(120\ s) \succ_w h(130\ s) \succ_w h(140\ s) \succ_w h(150\ s) \nsim_w h(160\ s) \succ_w h(170\ s) \nsim_w h(180\ s) \succ_w h(190\ s) \succ_w h(200\ s) \succ_w h(210\ s) \succ_w h(220\ s) \succ_w h(230\ s) \succ_w h(240\ s) \succ_w h(250\ s)$. With the exception of two transitions (from 150 s to 160 s and from 170 s to 180 s) a total order of the bubble size distributions in terms of weak submajorization predominates because of the strong sink (decreasing number of bubbles) in our system.

As one usually maps the structure of dependent on time statistical order (synonymous with the order of the classical majorization) of the normalized bubble size distributions by the Shannon entropy (Fig. 17), one can find maps which transform the order generated by weak submajorization on real values without changing its structure as well.

Therefore, choosing a function that preserve the order of the weak submajorization as in (7) given, see section 2, we can map the 'approximately' totally ordered bubble size distributions with $\sum_{i=1}^{10} p_i \leq 1$ on real values and obtain a monotonously decreasing function development for an increasing and Schur-convex function. For an increasing and Schur-concave function one obtains a monotonously increasing function development for the bubble size distributions with $\sum_{i=1}^{10} p_i \leq 1$.

In the following section 5 we investigate different functions in order to compare the influence of classical and weak submajorization on the description of the dynamics of the bubble size distributions.

5 Functions of the Majorization

In (19) a function is given which we call e_c-*function* (the index c is derived from the *c*lassical majorization). This e_c-function is normalized and maps distribution vectors $h(t) = (p_i(t))$ with $\sum_{i=1}^{n} p_i(t) = 1$ on the closed interval [0,1].

$$e_c(h(t)) = \frac{A - \sum_{i=1}^{n} \exp(p_i(t))}{A - n\exp(\frac{1}{n})}, \tag{19}$$

$$e_w(h(t)) = \frac{A - \sum_{i=1}^{n} \exp(p_i(t))}{A - n\exp(0)}, \tag{20}$$

$$\text{with} \quad A = \exp(1) + (n-1). \tag{21}$$

Additionally, this function is concave over the simplex S_{n-1} and fulfils the restrictions (22) and (23).

$$e_c(1, 0, \cdots, 0) = 0 \quad \text{on} \quad S_{n-1} \tag{22}$$

and in case of the equal distribution

$$e_c(1/n, \cdots, 1/n) = 1 \quad \text{on} \quad S_{n-1}. \tag{23}$$

Now for simplicity let $x = (x_i) \in \mathbb{R}^2$ be a distribution vector then

$$x_1, x_2 \in [0, 1] \qquad \text{and} \qquad x_1 + x_2 = 1. \tag{24}$$

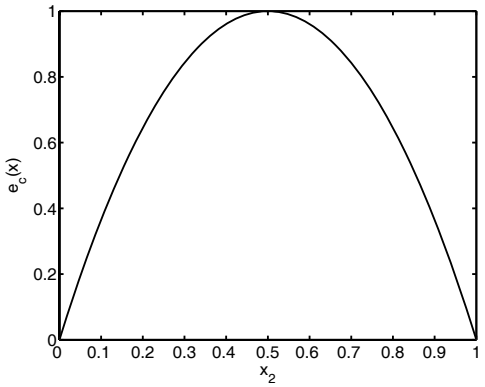

Figure 14: The e_c-function (19) that fulfils the restrictions in (22) and (23) on the simplex S_1. We see the e_c-function is Schur-concave and symmetrical that means permutations of the distributions vectors are mapped on the same real value (26).

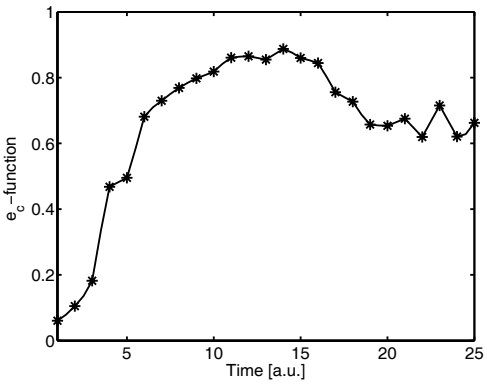

Figure 15: The time development of the bubble size distributions which are mapped on the interval [0,1] by the e_c-function (19). This function behaves like the Shannon entropy (17): at the beginning it increases and then it behaves irregularly.

Then

$$e_c(x) = e_c(x_1 = 1 - x_2, x_2) \tag{25}$$

and we can plot the e_c-function against $x_2 = 0, \cdots, 1$ and see in Fig. 14 the function is Schur-concave and symmetrical that means all permutations of a distribution vector are mapped on the same real value. Let x be a distribution vector and Q be a permutation matrix, then

$$e_c(x) = e_c(Qx). \tag{26}$$

The e_c-function maps the bubble size distributions on the interval [0,1] and similarly behaves like the Shannon entropy (17): at the beginning it increases and then it behaves irregularly when the rearrangement begins, see Fig. 17 and 15. It does not matter which Schur-concave function like the Shannon entropy (17) or the e_c-function (19) maps the bubble size distribution on the interval [0,1], the functional behaviour of the temporal development is preserved.

The function in (20) is similar to (19) except for the term in the denominator $n \exp(1/n)$, which becomes $n \exp(0)$ in (20). These terms $n \exp(1/n)$ and $n \exp(0)$ describe the final states (if $x = (x_i) \in \mathbb{R}^2$ then $x_1 = x_2$) and normalize the corresponding function. The final state of the classical majorization is the equal distribution ($x_1 = x_2 = 1/n = 0.5$) (23), (24) where the function e_c shows its maximum value. Therefore the term $n \exp(1/n)$ stands in the denominator of the e_c-function. The final state of the weak submajorization is $x_1 = x_2 = 0$,

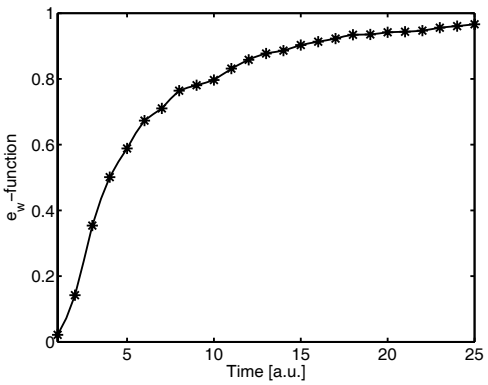

Figure 16: The time development of the bubble size distributions which are mapped on the interval [0,1] by the e_w-function (20). The functional development describes a continuously increasing function as we have mentioned in section 4.

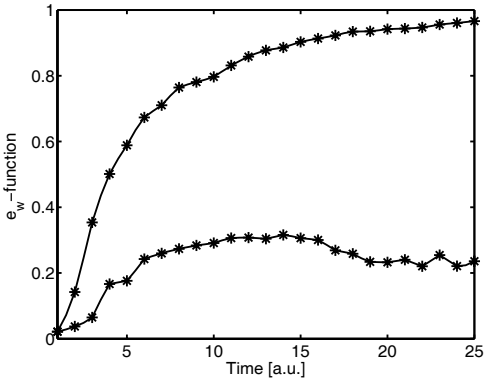

Figure 17: The time development of the normalized distributions (lower graph, compare to Fig. 15) and the non-normalized distributions (upper graph, compare to Fig. 16) which are mapped by the e_w-function (20) on the interval [0,1].

that means all objects have been eliminated and the corresponding function (20) shows its maximum value. Therefore we use the term $n \exp(0)$ in the denominator of (20). This function is called e_w-function (the index w is derived from *w*eak submajorization) and holds for distribution vectors with decreasing trace $\sum_{i=1}^{n} p_i \leq 1$, (7). (The simplex plot of the e_w-function (20) is discussed in section 5.1.) To apply the e_w-function to the absolute bubble size distributions (non-normalized number of bubbles of a certain size interval) one divides each absolute distribution by the sum of bubbles of the first absolute distribution (maximum number of bubbles). Then we obtain distributions with weak frequencies the sum of which is less equal than one: $\sum_{i=1}^{n} p_i \leq 1$. In Fig. 16 the time development of these distributions is shown which are mapped on the interval [0,1] with (20). This map by (20) describes a continuously increasing function as we have mentioned in section 4.

We take different functions (19), (20) for classical and weak submajorization to make the function development comparable (both functions are normalized to unity): Moreover, we can map the distributions with $\sum_{i=1}^{n} p_i = 1$ and the distributions with $\sum_{i=1}^{n} p_i \leq 1$ on the interval [0,1] with (20) too, since weak majorization contains classical majorization, (5) and (6). That means the e_w-function preserve the order of the classical majorization and weak submajorization expressed by (27).

$$\text{If} \quad y \prec x \quad \text{or} \quad y \prec_w x \quad \text{then} \quad e_w(y) \geq e_w(x). \tag{27}$$

In Fig. 17 we see the join of the graphs in Fig. 15 and 16 mapped by the

e_w-function (20).

Schur-concave functions as a measure to describe the statistical development of a sequence of distribution functions with $\sum_{i=1}^{n} p_i = 1$ or $\sum_{i=1}^{n} p_i \leq 1$ are discussed in detail. We know that such functions preserve the order of the majorization. All functions which belong to set of the Schur functions are suitable to describe such a distribution function development and only differ in the sign or the shape.

In an exemplary fashion, we like to show the time development of the bubble size distributions $h(t) = (p_i(t))$ which are mapped by a decreasing and Schur-convex function given by (28) [3]

$$S(h(t)) = \prod_{i_1 < \cdots < i_k} \sum_{j=1}^{k} p_{i_j}(t). \tag{28}$$

For simplicity we call it S-function. Only sums with $i_1 < \cdots < i_k$ are allowed and all these sums are multiplied to obtain real values of the S-function. Therefore, this function is not symmetrical that means it maps permutations of a distribution vector on different real values, (29).

$$S(x) \neq S(Qx). \tag{29}$$

x denotes a distribution vector and Q a permutation matrix. Consequently, we have to rearrange the bubble size distribution vectors $h(t) = (p_i(t))$ in decreasing order: $(p_1 \geq p_2 \geq \cdots \geq p_n)$ in order to apply this function (28) without contradictions.

For the S-function holds (30) and (31).

$$S(1, 0, \cdots, 0) = 1 \quad \text{on} \quad S_{n-1} \tag{30}$$

and for the equal distribution

$$S(1/n, \cdots, 1/n) = \frac{n!}{n^n} \quad \text{on} \quad S_{n-1}. \tag{31}$$

With (24) and $x_1 \geq x_2$ a simplex plot of $S(x_1 = 1 - x_2, x_2)$ versus $x_2 = 0, \cdots, 0.5$ can be shown in Fig. 18. Notice x_2 runs from 0 to 0.5 because the S-function is not symmetrical.

Now we come to our bubble size distributions $h(t) = (p_i(t))$. Both the bubble size distributions with $\sum_{i=1}^{n} p_i = 1$ and with $\sum_{i=1}^{n} p_i \leq 1$ can be mapped by (28) on the interval [0,1]. In Fig. 19 the upper graph describes the bubble size distributions which are normalized to unity. This graph monotonously decreases and then it begins to behave irregularly. The lower graph corresponds

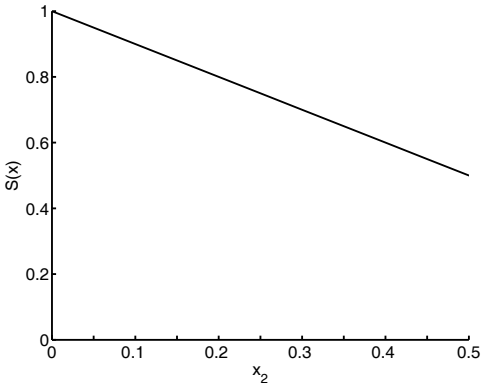

Figure 18: The simplex plot of the decreasing and Schur-convex S-function (28) with $x_1 \geq x_2$ and $x_2 = 0, \cdots, 0.5$ because the S-function is not symmetrical. This function fulfils the restrictions in (30) and (31).

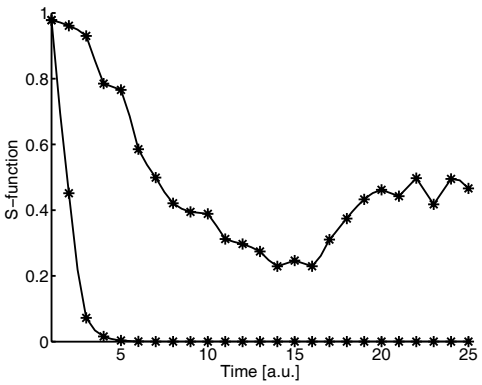

Figure 19: The time development of the normalized bubble size distributions (upper graph) and the non-normalized bubble size distributions (lower graph) mapped by the S-function (28) on the interval [0,1].

to the weak submajorization which takes into account a decreasing trace of the bubble size distribution vectors ($\sum_{i=1}^{n} p_i \leq 1$). This graph continuously decreases and converges against zero very fast.

This function (28) also preserves the order of the bubble size distributions like the e_w-function (20) however under changed conditions. The terms Schur-concave and Schur-convex differ in the sign that means Φ is Schur-concave if and only if $-\Phi$ is Schur-convex. Note that both these functions (S-function and e_w-function) and the Shannon entropy function (17) preserve the order of the classical majorization, but the latter does not fulfil (27) that means the Shannon entropy does not preserve the order of the weak submajorization.

5.1 Diffusion and Sink

Because of the inequalities (5) and (6) one may say that the classical majorization (2) and (3) is a subset of the weak majorization. The classical majorization describes the statistics of trace preserving distributions vectors (diffusion). The weak submajorization allows classical majorization and a trace decrease of the distribution vectors (sink). The last-mentioned mathematical relation characterizes both a diffusion and a sink. We like to give an approach to understand the connection between diffusion and sink more exact.

Firstly, we introduce a Δx to describe the sink. Let $x = (x_i) \in \mathbb{R}^2$ be a distribution vector with $x_1, x_2 \in [0, 1]$ and $x_1 + x_2 = 1$, (24). And let $\tilde{x} = (\tilde{x}_i) \in \mathbb{R}^2$ be a distribution vector with $\tilde{x}_1, \tilde{x}_2 \in [0, 1]$ and $\tilde{x}_1 + \tilde{x}_2 \leq 1$.

Then

$$x = \tilde{x} + \Delta x \quad \text{or} \quad \tilde{x} = x - \Delta x. \tag{32}$$

The $tr(\Delta x)$ can be defined by a real valued function $\Phi(x)$ and a strength factor α (strength factor α characterizes the strength of the sink). One can take any normalized real valued function $\Phi(x)$. For a simple approach we decided to take the normalized tent function (33) that we used in [6].

$$\Phi(x) = \left(1 - \frac{n}{2(n-1)} \sum_{i=1}^{n} \left| x_i - \frac{1}{n} \right| \right) \tag{33}$$

With a strength factor α a $tr(\Delta x) = \Phi(x)\alpha$ can be reformulated in (34)

$$tr(\Delta x) = \left(1 - \frac{n}{2(n-1)} \sum_{i=1}^{n} \left| x_i - \frac{1}{n} \right| \right) \alpha \quad \text{with} \quad 0 \leq \alpha \leq 1. \tag{34}$$

Considering (34) for $x = (x_i) \in \mathbb{R}^2$ one obtains a Δx_i for x_1 and x_2:

$$\Delta x_i = (1 - 2|x_i - 0.5|)\alpha \quad \text{with} \quad 0 \leq \alpha \leq 0.5 \tag{35}$$

$$\text{and} \quad \Delta x_1 = \Delta x_2, \quad \Delta x_1 + \Delta x_2 = tr(\Delta x). \tag{36}$$

Generally,

$$\sum_{i=1}^{n} \Delta x_i = n \Delta x_i = tr(\Delta x). \tag{37}$$

If $\alpha = 0$ we obtain the classical majorization (no trace changing, since $tr(\Delta x = 0)$) and $\alpha = 0.5$ describes a pure weak submajorization (that means a predominate sink and a hardly distinctive diffusion) with the final state $\tilde{x}_i = 0$.

As an illustration the S_1 simplex plot for the symmetrical e_w-function (20) with a Δx can be generated. Then

$$e_w(\tilde{x}) = e_w(x_i - \Delta x_i) \tag{38}$$

and Δx_i is given by (35).

In Fig. 20 both extreme cases $\alpha = 0$, $\alpha = 0.5$ and the case $\alpha = 0.25$ are given. The plot for all $\alpha = 0, \cdots, 0.5$ would fill the area between the both graphs of $\alpha = 0$ and $\alpha = 0.5$ in Fig. 20. Conspicuously, the continuous graph of $\alpha = 0$ develops with increasing α a graph on the simplex S_1 that is not continuously differentiable. We see a vertex at $x_i = 0.5$ for $\alpha > 0$.

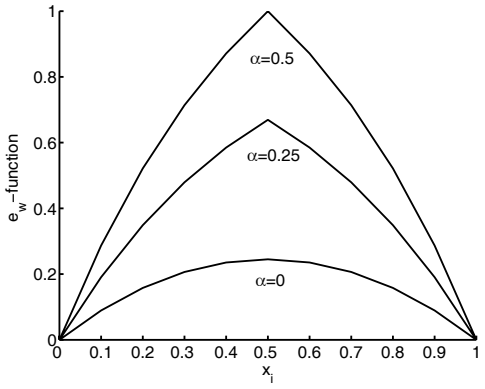

Figure 20: The e_w-function on the simplex S_1. Both extreme cases can be seen: the classical majorization with $\alpha = 0$ (lower graph) and the weak majorization respectively weak submajorization with $\alpha = 0.5$ (upper graph). Additionally, the graph of $\alpha = 0.25$ (middle) is given.

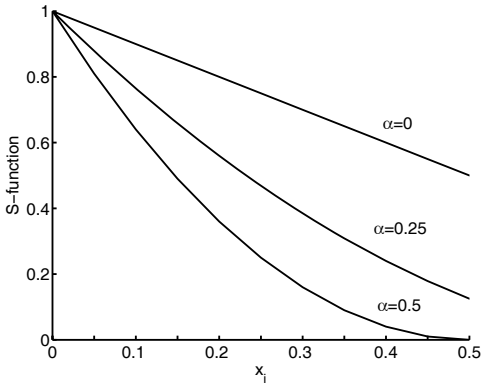

Figure 21: The S-function on the simplex S_1. Both extreme cases can be seen: the classical majorization with $\alpha = 0$ (upper graph) and the weak majorization respectively weak submajorization with $\alpha = 0.5$ (lower graph). Additionally, the graph of $\alpha = 0.25$ (middle) is given.

Just as in the same manner the e_w-function we can plot the S-function (28) with

$$S(\tilde{x}) = S(x_i - \Delta x_i). \tag{39}$$

Notice that the simplex plot runs from $x_i = 0$ to $x_i = 0.5$, because the S-function is not symmetrical (29). Fig. 21 shows the graphs of the classical $\alpha = 0$ and the weak majorization $\alpha > 0$.

In this section 5 majorization ordering preserving functions describe our bubble size distribution dynamics in various ways. It all depends on the normalizing of the distribution or in other words it depends on the mathematical relations, classical majorization or weak submajorization. Due to the foam decay process, we considered a diffusion process with a sink term with a variable strength α and therefore we prefered the weak submajorization. The weak majorization enables us to describe a sequence of distribution functions where the number of objects is not necessarily an invariant.

6 Conclusion and Outlook

On the basis of Ruch diagram lattices [5] we can clearly illustrate the classical majorization and weak submajorization. Additionally, the ordering of the diagrams can be influenced by normalizing, by the number of size intervals and by

permutations. Refering to our bubble size distributions it makes a big difference whether we use the classical or the weak submajorization represented by different functions that preserve the ordering of these mathematical relations.

The classical procedure by means of normalizing the bubble size distributions and using the Shannon entropy leads to a separation of two processes of the foam decay [8]: drainage (increasing Shannon entropy) and rearrangement (irregular behaviour of the Shannon entropy). However, the decreasing number of bubbles during foam decay is not taken into account. The weak submajorization offers a common characterization of diffusion and sink (decreasing number of bubbles). The continuing diffusion with sink corresponds to a monotonously increasing or decreasing function that preserves the order of the weak submajorization.

In summary, one can say, the quantitative comparison of orderings requires a map of these structures on real values like the Shannon entropy maps the order of the classical majorization on real values. We have shown by the introduction of the weak majorization that functions can be found which map systems with variable number of objects on real values so that the order is preserved and a measure can be found.

Additionally, we have successfully introduced a strength of sink and diffusion by the factor α. It would be interesting to consider the temporal development of this factor α of the real bubble size distributions.

In this context it becomes meaningful to introduce a weight factor for Δx_i. Up to now, only Δx_i with equal weights have been formulated for the 2-dimensional space. A possible weighting function is given by (40)

$$n\Delta x_i = \sum_{i=1}^{n} \beta_i \Delta x_i = tr(\Delta x). \tag{40}$$

In section 3 we have discussed the influence of varying row number or dimension for partition diagrams. Therefore it would be helpful to find an objective criterion for optimal bin width selection for our system. This criterion should refer to the number of size intervals.

Moreover, an interesting point is the fact that each transition of the weak submajorization can be expressed by a doubly substochastic matrix. The generation of these matrices will be discussed in our next paper.

References

[1] P.M. Alberti, A. Uhlmann, *Dissipative Motion in State Spaces*, Teubner Texte zur Mathematik Bd. 33, Leipzig, (1981).

[2] G.H. Hardy, J.E. Littlewood, G. Polya, Inequalities, Cambridge University Press, London (1934).

[3] A.W. Marshall, I. Olkin, *Inequalities: Theory of Majorization and Its Applications*, Academic Press, (1979).

[4] R.F. Muirhead, *Some methods applicable to identities and inequalities of symmetric algebraic functions of n letters*, Proc. Edinburgh Math. Soc. **21** (1903), 144–157.

[5] E. Ruch, *The Diagram Lattice as Structural Principle*, Theoret. Chim. Acta (Berl.) **38** (1975), 167–183.

[6] S. Sauerbrei, E.C. Hass, P.J. Plath *The Apollonian Decay of Beer Foam - Bubble Size Distribution and the Lattices of Young Diagrams and their Correlated Mixing Functions* , Discrete Dynamics in Nature and Society, Volume 2006, Article ID 79717, 1–35.

[7] S. Sauerbrei, U. Sydow, P.J. Plath *On the Characterization of Foam Decay with Diagram Lattices and Majorization*, Z. Naturforsch. A **61 a** (2006), 153–165.

[8] S. Sauerbrei, P.J. Plath, *Diffusion Without Constraints*, Journal of Mathematical Chemistry, DOI: 10.1007/s10910-006-9085-x (2006).

[9] C.E. Shannon, *A Mathematical Theory of Communication*, The Bell System Technical Journal, Vol. **27**, (1948) 379–423, 623–656.

[10] H. G. Zachmann, *Mathematik für Chemiker*, VCH, Weinheim, 1994.

Received: October 4, 2006